39th AIAA Fluid Dynamics Conference
22 - 25 June 2009, San Antonio, Texas

AIAA 2009-4303

POD Analysis of 3-D Flow Visualization Images of a Circular Jet with Reynolds Number 9500

Kyle P. Lynch* and Brian S. Thurow†
Advanced Laser Diagnostics Laboratory
Department of Aerospace Engineering
211 Davis Hall
Auburn University, Auburn, AL 36849

A three-dimensional (3-D) modal analysis of an excited circular jet with Reynolds number of 9500 is conducted using proper orthogonal decomposition (POD) and a high-speed 3-D flow visualization system. Large sets of 3-D data are acquired in the near field before the end of the potential core and the transition region of the jet. POD is used to objectively characterize and classify the 3-D images and elucidate the fundamental structure of the flow. As expected, the near field of the jet is dominated by the formation and growth of ring vortices, which is also reflected in the shape of the POD modes. The onset of azimuthal instabilities is also clear in the instantaneous 3-D images, which show long streamwise fingers, or side jets, of fluid surrounding the vortex rings. The results presented here show the strength of 3-D modal analysis for understanding the most dominant structures and instabilities in the jet.

I. Introduction

Jets are an excellent platform for the study of fluid dynamics and turbulence as they display numerous phenomena that are encountered throughout the field of fluid dynamics. Topics represented include instability, receptivity, vortex dynamics, transition, coherent structures and fully developed turbulence. As these features present themselves and develop with increasing distance from the jet nozzle, a jet flow field is convenient for the in-depth study of any of these topics by making measurements at the appropriate location downstream of the nozzle exit. In a previous study conducted by our laboratory, we presented our efforts using a unique 3-D flow visualization system and the proper orthogonal decomposition to study the physics of transition to fully developed turbulent flow in an axisymmetric jet without artificial excitation [see Ref. 1]. This work was preliminary in nature and mainly geared as an educational exercise for the development of a 3-D flow visualization system. The lessons learned conducting the experiment and in data processing, completion of substantial upgrades to the 3-D visualization system, as well as the desire to study the flow field in additional detail has led us to revisit the topic in an expanded study. This effort maintains the same primary focus, but represents a more detailed analysis using larger data sets (650 3-D images vs. 350 in the previous study) and more mature image processing steps developed for 3-D flow visualization. Presented here are our preliminary results of this new and expanded study.

In addition to improvements in the 3-D flow visualization process, key differences from the earlier work are the use of smoke (instead of small water droplets) as a flow tracer and an increase in Reynolds number from 6800 to 9500. As discussed in Dimotakis [2], a Reynolds number of 10,000 roughly represents a critical point beyond which the far field of a jet can be considered as capable of generating fully developed turbulence and the effects of further increasing Reynolds number become diminished. As such, an understanding of the fundamental physics that govern this change are quite important.

Jets have received considerable attention over the last several decades [see Refs. 3-22 for a small sampling of the literature available on the subject]. Briefly, a jet's flow field can be summarized as follows. The flow at the exit of the nozzle is uniform at the jet centerline with a region of shear near the wall. Upon exiting the nozzle, the shear layer with thickness, θ, is susceptible to the Kelvin-Helmholtz, or shear-layer, instability where small disturbances, typically characterized by their Strouhal number ($St_\theta = f\theta/U$), are amplified and eventually roll up into organized and quasi-periodic sets of vortices. Further shear layer growth is dominated by the dynamics of these vortices and

* Graduate Research Assistant, Student Member AIAA.
† Assistant Professor, Member AIAA. Corresponding Author: thurow@auburn.edu

described by events such as vortex pairing. As the vortices grow and move towards the end of the potential core, the dominant jet instability mode becomes that of the preferred mode, or jet column mode, which is characterized by the Strouhal number based on the nozzle diameter (St_D = fD/U). The vortex itself is also subject to an azimuthal instability that can lead to the formation of structures defined by their azimuthal wavenumber. Near the end of the potential core and beyond, the interaction of vortices leads to complex non-linear motion that destroys the organized motion of vortices in the flow and results in the transition to turbulence. Many jet diameters further downstream the flow is well described as fully developed turbulent flow.

The development of the flow beyond the potential core, however, has received considerably less attention. In this region, the well organized structure present near the nozzle exit diminishes as the flow is governed by non-linear dynamics and eventually breaks down into fully developed turbulence. As the flow in this region of the jet is highly unsteady and three-dimensional, it is much more difficult to investigate. Classically, it has been assumed that the far field pattern of the jet is self-similar and independent of the initial disturbances provided. Experiments on bifurcating and blooming jets, however, show that the far field flow can be dramatically altered through the proper introduction of disturbances at the jet exit [19]. These experiments suggest that different far-field turbulent states are possible for a given geometry. This alteration of the far field is directly connected the near-field vortex structures created by the disturbances and the dynamics of these vortices as they undergo the transition to turbulence.

These observations incite a number of fundamental questions about fluid dynamics and turbulence. For example: Is turbulence truly independent of the initial conditions that led to it? How long, or over what length, does it take for the flow to fully transition to fully developed turbulence? What are the physical mechanisms responsible for this transition? Can we manipulate or exploit these mechanisms to achieve different turbulent states, perhaps for a practical benefit? These questions are not new to the field of turbulence and have been debated extensively over the past century. From a practical point of view, the answers to these questions are very important and worthy of additional exploration. We must consider the fact that numerous engineering applications are characterized by transitional flows and that fully developed turbulence is only reached in the limit. In addition, once a flow is fully turbulent, flow control becomes much more difficult as actuators must overcome the strong fluctuations and turbulent energy already present in the flow. More efficient control might be possible through manipulation of the transition process such that the turbulence initially develops with the characteristics suited for the application. While transition has been the focus of numerous research efforts, the problem remains challenging due to the three dimensional, unsteady and non-linear nature of the flow field and the equations that describe it.

In this work we apply a recently developed high-speed 3-D flow visualization system to interrogate the 3-D characteristics of large scale structures in an axisymmetric jet as it transitions to turbulence. A follow-on study is planned where we will use acoustic excitation to excite the jet and compare to the baseline case of flow without excitation. The ability to acquire 3-D images of the flow during the transition process is a relatively new capability developed recently in our laboratory. 3-D flow visualization provides us with a unique tool to visualize, follow and characterize large-scale structures in more detail and depth than possible before.

Our main data analysis tool, besides looking directly at the 3-D flow visualization images, is the proper orthogonal decomposition (POD). POD has found many uses in the fluid dynamics community, particularly with respect to flow control applications, where the prospect of forming a low-dimensional model for seemingly complex and highly dimensional flow fields is quite attractive. In this work, we use POD as a means of objectively classifying and describing the flow field under observation. POD has been described in great detail elsewhere [e.g. Refs. 23-28] and a complete description is beyond the scope of this paper. For our purposes, we are interested in the ability of POD to objectively decompose an ensemble set of data into its fundamental set of modes. These modes are optimal in the sense that the energy of the flow (or variance in the case of flow visualization images) converges faster when projected on these modes than any other possible set of modes. As such, POD modes are thought to represent the largest and most energetic structures of turbulence. We utilize the snapshot method to form POD modes of large sets of 3-D images. As such, each POD mode is also 3-D. We emphasize that POD is not be used here to form a reduced order model for flow control purposes, but, rather, is being used here as a tool to aid in the analysis of complex 3-D images.

II. Experimental Arrangement

The jet facility consists of a converging nozzle attached to a settling chamber. A 10" diameter speaker is mounted on the floor of the chamber to allow for acoustic excitation, a capability we plan to explore in the near future. Seed particles are generated in a secondary chamber using a smoke machine to create small smoke particles that are mixed with the air flow delivered to the nozzle. A fan is used to force the smoke particles and air through a 2" diameter hose and into the settling chamber. Honeycomb and a perforated plate are located at the inlet to the nozzle for flow conditioning. The nozzle has a contraction length of 6.5" and an exit diameter of 1.2". The current particle seeding arrangement represents a change from the experiments conducted in Ref. 1; previously, an ultrasonic water mister was used to generate small water particles for seeding. However, an effort to characterize the performance of these particles concluded the Stokes number of the particles was far too high (≈1.8, based on a particle diameter of approximately 78 microns), for the particles to faithfully follow the flow. Additionally, evaporation of the particles would occur, leading to substantially reduced signal levels in the far field images.

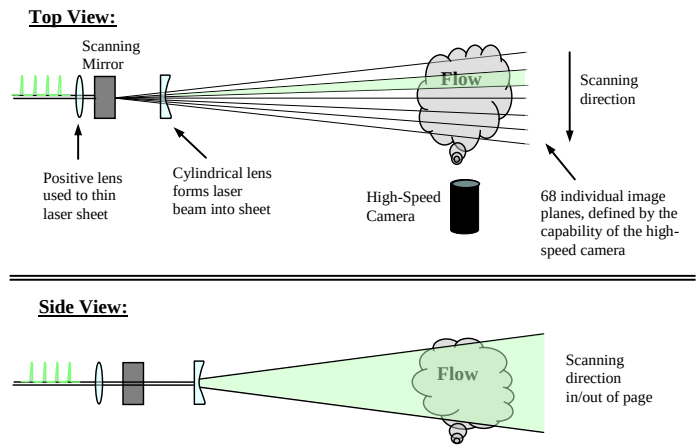

Figure 1. Schematic of Laser Sheet Scanning Technique

The flow exiting the nozzle is illuminated using a thin laser light sheet. In this fashion, the interface between the jet fluid (seeded with small smoke particles) and the ambient is visualized with the presence of vortex structures in the shear layer being quite apparent. Mixing between the seeded jet fluid and unseeded ambient fluid results in a reduced intensity that is also visible in the images. 3-D flow visualization is accomplished by scanning the laser sheet through the flow field and acquiring 2-D images of the flow throughout the scan, as shown schematically in Figure 1. The resulting sequence of 2-D images can then be reconstructed to form a 3-D image of the flow field. The unique aspect of this work is the high-speed capabilities of the technique, which are made possible using a MHz-rate pulse burst laser, a galvanometric scanning mirror and a high framing rate CCD camera. A detailed description of the technique can be found in Ref. 29.

The main piece of instrumentation used in the technique is a home-built pulse burst laser system that is capable of producing laser pulses at repetition rates in excess of 1 MHz over a ~1 msec long window [31]. Recently the laser system has been significantly upgraded with two additional laser amplifiers, enabling the system to generate 20 nsec duration pulses containing approximately 10 mJ per pulse at 532 nm at 500 kHz repetition rates. A substantial portion of this upgrade was the inclusion of a phase conjugate mirror (PCM), sometimes referred to as a stimulated Brioullin scattering (SBS) mirror, as the double pass mirror in amplifier 3. This is an optical cell filled with carbon disulfide liquid, which is a nonlinear optical medium that acts as a low-pass filter, preventing low-intensity noise from propagating further in the amplifier chain, thus improving the efficiency and achievable pulse energy of the laser system. Additionally, beam quality is improved through the phase conjugation properties of the process and propagation back through the third amplifier [see Ref. 32 for more background on CS_2 and its use as a PCM].

Unfortunately, an electrical failure in the power supply of amplifier 4 prevented the laser from operating at maximum power in this work. It is estimated that after repairs are made to the unit and it is integrated back into the system, a pulse energy at 532 nm of over 25 mJ/pulse will be attainable. For 3-D flow visualization, a burst of 68 laser pulses is produced at a 500 kHz repetition rate and deflected off of a 6 mm aperture galvanometric scanning mirror. A long focal length spherical lens located in front of the scanning mirror and a cylindrical lens placed immediately after the scanning mirror is used to form an approximately 150 μm thick laser sheet whose position is determined by the momentary angle of the scanning mirror. The speed of the mirror can be adjusted to yield different scan lengths with each sheet being uniformly distributed along the scan direction. Images are acquired for each successive laser pulse using a DRS Hadland Ultra68 intensified camera. The Ultra68 is capable of acquiring 68 images with 220 x 220 pixel resolution at framing rates up 500,000 frames per second. Thus, a sequence of 68 images can be acquired in 136 microseconds.

Multiple image corrections are applied to the resulting image sequences to reduce the effect of camera noise and to account for changes in the field of view of the camera during the scan. A flat field correction is first performed internal to the camera manufacturer's software, which neutralizes bulk fluctuations in signal values by imaging a

target with uniform illumination and creating a set of correction coefficients to apply to subsequent image sequences. Note, the camera used in this study is inherently noisy, and has large pixel-to-pixel random fluctuations of the flat field on the order of 8%. A dark field subtraction is performed next to eliminate a constant, low-level CCD noise that is not eliminated with the flat field correction. After that, a correction for an image artifact issue (termed "ghosting") is applied. This ghosting refers to an effect where a small portion of a particular image in a sequence will bleed over into the remaining images. A correction matrix has been created utilizing a laser sheet scan to determine the ratios of bleed over for each image. By taking the inverse of this correction matrix and applying it to each complete image sequence, the effect of the bleed over is reduced. The laser line scan technique is a first attempt at a highly accurate ghosting correction, and efforts are currently underway to further improve this correction.

Next, a thresholding is performed, setting image values under a certain threshold to zero. The following images are then normalized to correct for bulk variations in image intensity due to seeding levels, and a non-uniform laser sheet intensity profile. After this, a 3 x 3 x 3 3-D median filter was applied. Median filters are excellent for reducing small-scale noise while preserving and enhancing edges. Since the primary focus of this study relies on the delineation between jet fluid and the ambient fluid, the median filter well matches the needs of the study. The final correction performed is a spatial calibration, which corrects for the change in field of view across the scan. A dot card is placed at the front and back of the scan and imaged. Using MATLAB image transformation functions, each image is individually corrected for the depth of field.

One of the conclusions reached in the current study is that these corrections have a strong influence on the calculation of POD modes. The POD modes represent the structure of any fluctuations in intensity, whether naturally or artificially produced. Due to the nature of the 3-D flow visualization technique where pulse energies can fluctuate from pulse to pulse and within the laser sheet itself, the presence of artificial intensity gradients become more pronounced. Thus, the goal is to come up with a scheme that emphasizes the natural features of the jet and mitigates artifacts due to the image process. This process is currently being refined.

III. Experimental Results

A. Near-Field Jet Structure

Each 3-D image consists of 220 x 220 x 68 pixels of intensity data. 3-D images were first formed in Matlab and then displayed using TecPlot, a software package designed for visualization of CFD and numerical results. We present data in several formats including iso-surface plots, cross-sectional exploded assembly views and 2-D image slices. In addition, color is used heavily to add contrast to the images. Due to this, it is recommended that the reader view this paper on a computer so that images can be viewed in color and scaled to the appropriate size for easy viewing.

1. Instantaneous Images

Figures Figure 2 and Figure 3 show two iso-surface views of two different instantaneous 3-D images acquired in the near-field of the jet. The scan direction corresponds to the z-axis in all of the figures presented. Impressively, the scan direction is difficult to determine from the visualizations, although some striations are visible when approaching tangency to the jet exit and other structures.

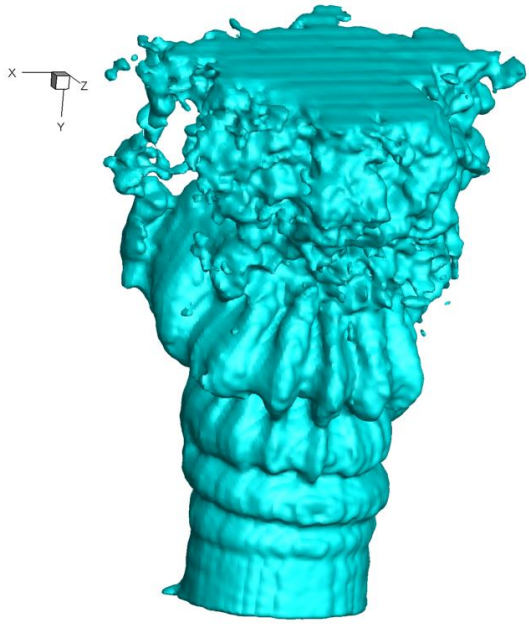

Figure 2. Isosurface Rendering of Near Field Jet 3-D Flow Visualization Data

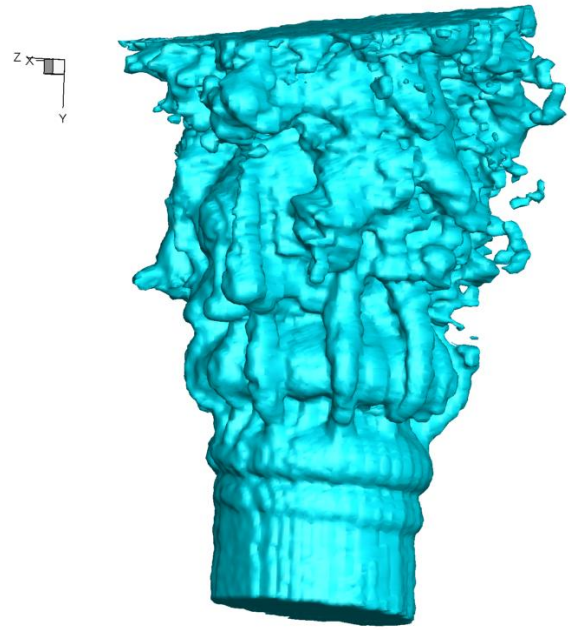

Figure 3. Isosurface Rendering of Near Field Jet 3-D Flow Visualization Data

In general, iso-surfaces give an aesthetically pleasing 3-D view of the flow field, but the opaque surface masks the additional information available in these images. Exploded views showing various cross-sections help fill in the missing details. In Figure 4, the y axis has been stretched to allow full viewing of each cross-section. 10 cross-sectional slices (out of a possible 220) are shown with each cross-sectional image having a resolution of 220 x 68. It should be noted that these slices (x-z plane) do not correspond to the original 2-D images (y-z plane) from which the 3-D images were reconstructed.

Images acquired in the near field span from 0.15 jet diameters to 3.125 jet diameters downstream. In this region, the flow is dominated by the formation and growth of large-scale ring vortices that arise from the instability of the shear layer near the nozzle exit. The presence of these ring vortices is apparent in Figures Figure 2 and Figure 3. The most striking features of these images, however, are the presence of azimuthal instabilities on the vortex rings. Near the nozzle exit, the cross-sectional view shows the jet as being round; however, further downstream, the growth of azimuthal instabilities becomes apparent. In the reconstructed image of Fig. 2, these instabilities take the form of elongated fingers of fluid that surround the jet with a quasi-periodic structure in the azimuthal direction. Examination of the images indicate that the azimuthal wavenumber corresponds to higher order modes up to m=20 (see Fig. 2), which is significantly higher than we had expected. A more comprehensive literature search is underway to better understand these observations.

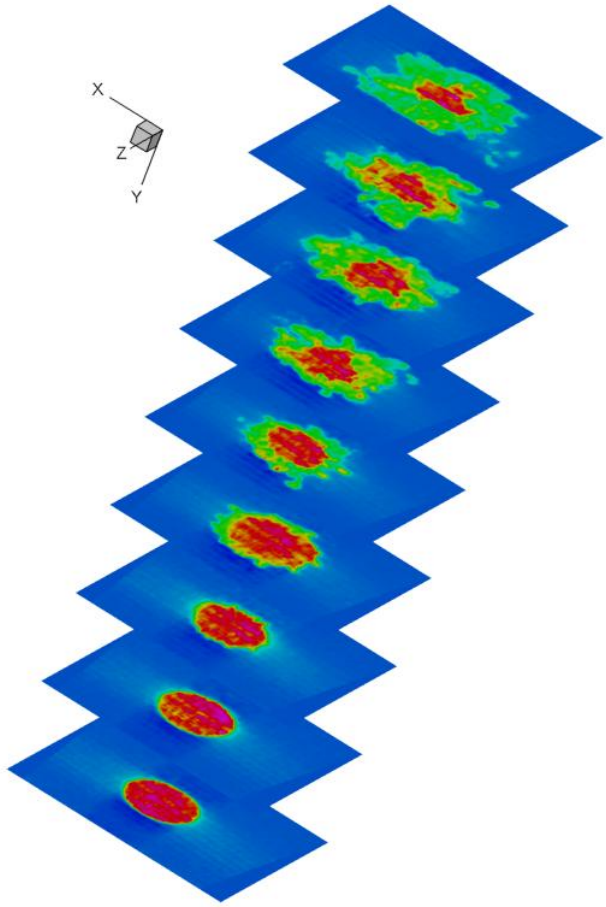

Figure 4: Exploded cross-sectional view of 3-D flow visualization of the jet in the near-field region. The bottom slice is at y/D = 0.15 and top slice is at y/D = 3.125

2. 3-D POD Modes

POD was applied to the full set of images in order to determine the most energetic modes of the flow. One problem encountered in this work was maintaining a constant seeding level using the smoke machine. A full set of images took many hours to acquire and the level of smoke had to be manually monitored and controlled. This resulted primarily in changes to the mean pixel values of each image, as the spatial resolution of each pixel was far larger than the particle size, and thus integrated the scattered signal from many particles. A normalization of the entire data set by the mean value of each 3-D image yielded an approximate correction for these fluctuations. A commercial smoke machine with precise smoke output control has been ordered and will be used in future works to mitigate this effect.

A problem encountered in a previous effort was a slow drift of the measurement volume along the scan direction which was found to be due to a thermal dependence of a magnetic encoder embedded in the scanning mirror, causing the position of the deflected laser sheets to move relative to the jet axis. A new scanning mirror and servo controller was used in this study (GSI Lumonics VM500+ / GSI Lumonics MiniSAX II) that includes an optical encoder. Use of this new mirror has shown no thermal drift over the length of time needed to acquire an entire data set. This was verified by examining cross-stream slices near the jet exit over the course of the experiment.

The POD modes presented here display some interesting features about the flow and show significant promise for future 3-D data analysis efforts. The distribution of energy across the POD modes is concentrated heavily onto the first few modes. For flow visualization images, energy refers to the variance in image intensity as opposed to a true energy of the flow. Thus, the modes can be thought of as representing a decomposition of the image intensity into a set of mode. The energy quickly converges to less than 1% by mode #20. To put this in perspective, if the 650 images that comprise the data set were completely random and uncorrelated, then all modes would represent approximately ~0.15% each of the total energy.

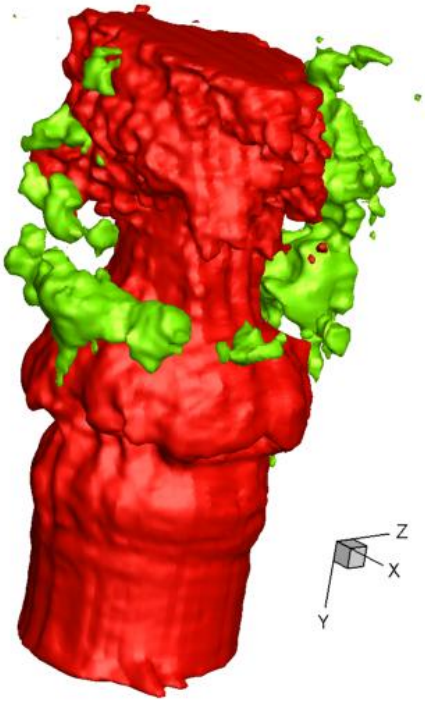

Figure 5: Isosurface Visualization of Near-Field Mode 1

The first POD mode is shown in Figure 5. This mode shows a large positive value filling the location of the jet core, with negative values surrounding a large ring around y/D = 2. We suspect this mode to be an artifact of laser sheet intensity normalization. In the majority of the images, the highest intensities were found to occur near the same region. The per-image normalizations would thus introduce a variance in this region, which is reflected prominently in this mode. Various other normalizations methods will be utilized in the future, in the effort to have the first POD mode represent a purely fluid dynamic phenomena rather than an experimental or data processing artifact. However, we do examine the remaining modes which reveal very interesting flow structure. As discussed earlier, we are in the process of refining our image processing steps to avoid these types of errors.

Figure 6 shows modes 2 through 7 using both iso-surface plots and more conventional 2-D slices through plane 34 (out of 68; this represents the center slice). The 2-D slices have the advantage of showing greater internal details about the modes that often is occluded by the iso-surface visualization.

Mode 2 and 3 clearly represent the quasi-periodic formation and growth of vortex rings throughout the near field. The alternating colors represent positive and negative values; thus these modes also give some insight into the spacing between periodic vortex rings. Also interesting is how mode 3 appears to be "phase-shifted" from mode 2, i.e., the positive and negative values flip from mode 2 to 3. This is an indication that the precise downstream location of vortex formation is different between individual images and can be described by an overlay of these two modes.

Higher-order modes begin to exhibit greater three-dimensional effects and in some cases breakdown of symmetry about the jet axis. Very near the jet exit, mode 4 is similar to the previous modes in describing vortex ring formation. Further downstream, the mode begins to describe a possible "flapping" motion, where positive values opposite to each other and negative values in the jet center indicate the jet has a tendency to deviate to either of the positive directions. Similar and opposite behavior is seen in mode 6; the orientation of the iso-surface is unchanged, however the values appear to be rotated 90 degrees about the jet centerline, allowing an additional degree of freedom for the jet to "flap" perpendicular to the motion described in mode 4. Mode 5 appears to describe an azimuthal instability that creates waves in the vortex rings and leads to the creation of streamwise "fingers." This behavior has been seen extensively through individual images in the data set. It is possible that many strong repeating features are being captured in the first mode, but are being dominated by the variance caused by normalization procedures. Still, the information contained in these modes is quite promising.

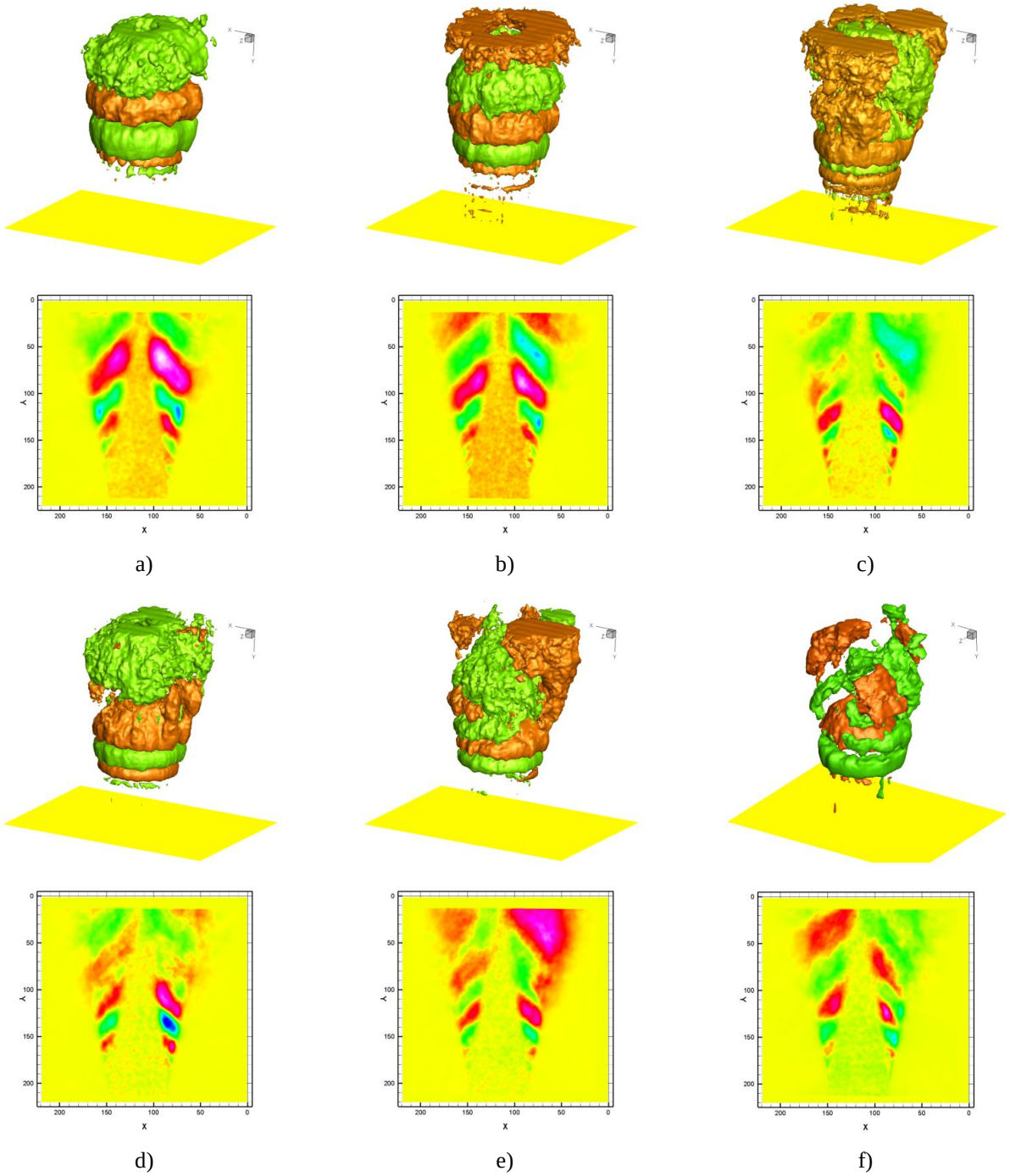

Figure 6. 3-D Iso-surface and 2-D central plane slice visualizations of near-field POD modes. a) mode 2, b) mode 3, c) mode 4, d) mode 5, e) mode 6, f) mode 7. The colormaps are matched for the 3-D isosurface and the accompanying 2-D slice.

Higher-order modes 10, 25, and 50 are shown in a streamwise cross-sectional view in Figure 7. The scale of the structures captured in these modes is much smaller than those captured in the first few modes, and thus iso-surfaces become less-effective at conveying the internal structure. In each of the modes presented, azimuthal instabilities that are along the entire length of the near-field appear to dominate. This is visualized by the alternating positive and negative values along the outer diameter of the jet. Again, these instabilities are clearly seen in individual images. Therefore, these modes act to account for various azimuthal mode numbers and instability amplitudes.

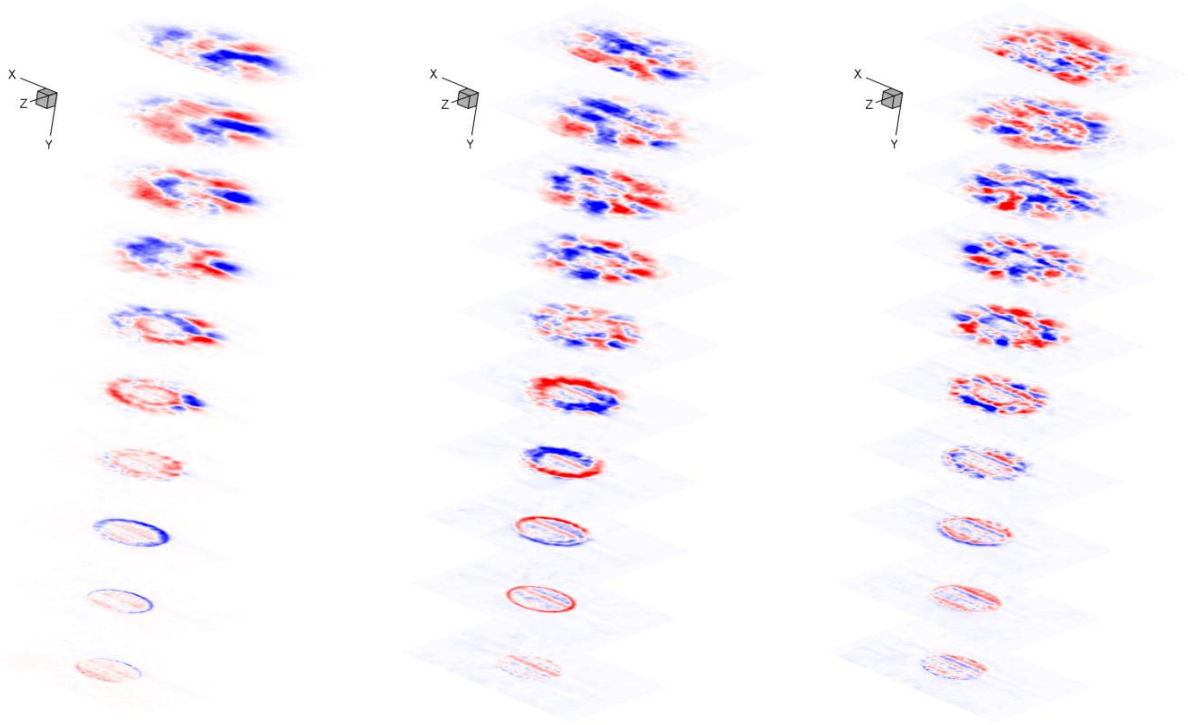

a) b) c)

Figure 7. Exploded cross sectional views of a) mode 10, b) mode 25, c) mode 50.

B. Transition Region Jet Structure

One of the long-term goals of this work is to construct a detailed picture of the transition of a jet flow from quasiperiodic ring vortices in the near field to the fully developed turbulence in the far field. As such, a large set (650) of images was acquired between 3.25 and 7.0 jet diameters downstream. This location is centered on the end of the potential core in a region where ring vortices do not provide a good description of the flow. In this region of the flow field, the vortex rings produced near the nozzle exit have spatially grown and become more unstable. The size of these rings is large enough to cause interaction of a single vortex ring with itself. This results in a rapid breakdown into turbulent flow.

1. Instantaneous Images

Figure 8: Sample 3-D flow visualizations of the jet in the transition region. An iso-surface is used to represent the jet fluid, with a cutaway displayed using a 2-D slice. shows a combination iso-surface and 2-D slice view of the jet in the transition region. Additional difficulty lies in visualizing the transition region data, due to the smaller scales of turbulence present in the flow. Thus, an isosurface typically does not reveal a great deal of information about the flow. Rather, slices or cutaway views allow investigation into the internal structure of the flow while still providing spatial context. The intensity values in the images do however provide information on jet mixing that is not extensively noticeable in the near-field set. The bright regions in the image correspond to unmixed jet core fluid, due to the greater number density of particles in these regions. The remaining lower intensity regions are due to mixing of the jet fluid with ambient fluid, which results in a lower number density of particles, and thus reduced

scattered signal. In this way, the behavior of the core fluid can be analyzed separately, but with complimentary information provided by the large mixing layer.

Of note is a change in the shape and size of large scale structures as were seen before in previous work at a lower Reynolds number and using water particles for seeding. We believe both these factors to substantially influence the behavior of the jet in this region. As mentioned before by Dimotakis [2], flows must approach a Reynolds number of approximately 10^4 in order to support of fully-turbulent flow. Here the downstream distance from the nozzle is too small to consider the turbulent flow to be fully-developed, however Reynolds number effects are also important in the transition region. In this sense, the lack of large scale structures as seen previously is an indication that this criterion is being approached. The previous use of water particles also may have contributed to the formation of large scale structures due to the large particle diameter and settling velocity measured. These particles could not faithfully follow the small-scale flow evident in this region.

Figure 9: A cross-sectional view of the jet in the transition region. presents a cross-sectional view of the jet transition region. This provides another perspective on the turbulent transition, presenting a clear breakdown of jet centerline axis symmetry.

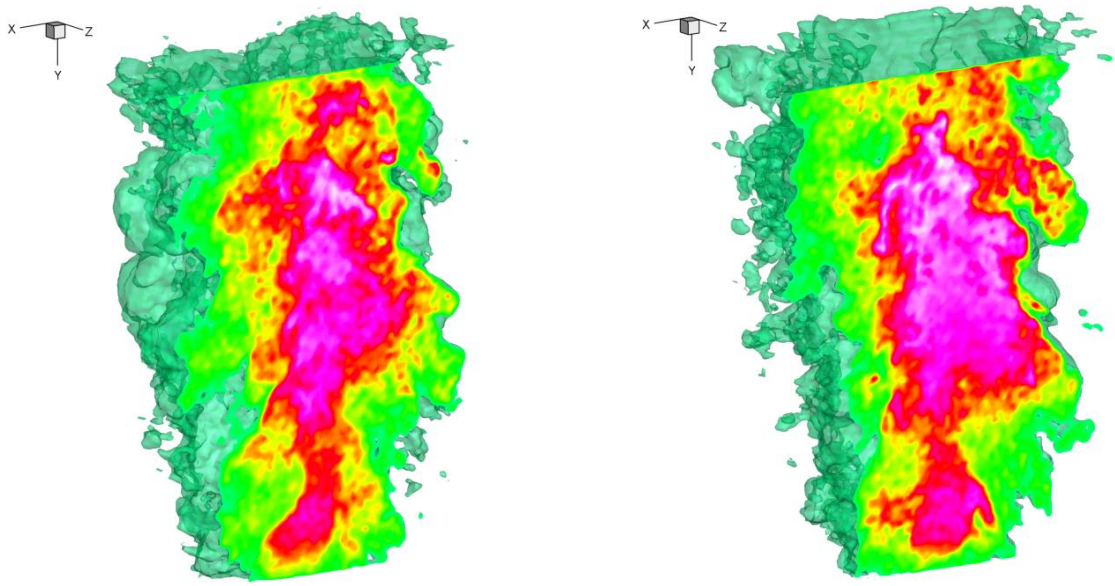

a) b)

Figure 8: Sample 3-D flow visualizations of the jet in the transition region. An iso-surface is used to represent the jet fluid, with a cutaway displayed using a 2-D slice.

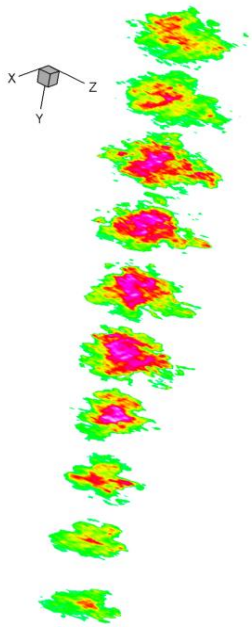

Figure 9: A cross-sectional view of the jet in the transition region.

2. 3-D POD Modes

The visualizations presented above provide an interesting insight into the flow structure; however, analysis of these images themselves is complicated by the smaller spatial scales involved and by the general pseudo-random and chaotic nature of turbulence itself. These factors necessitate the use of POD to objectively characterize the large amount of data contained in each image sequence and the 650 image sequences taken as a whole.

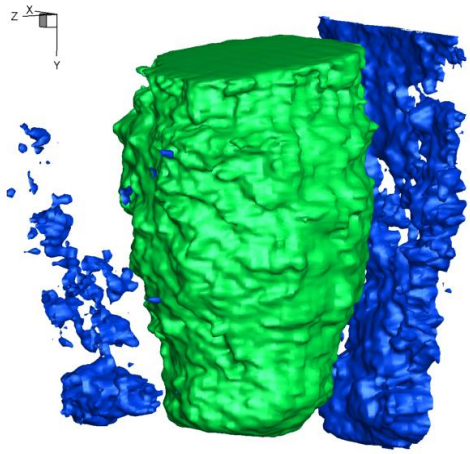

Figure 10: POD Mode 1 of the transition region.

The first POD mode is shown in Figure 10. Similar to the first mode in the near field, the structure seen here seems to represent normalization procedures. Again, normalization will be revisited, and the goal is to have the first mode directly represent a fluid phenomena.

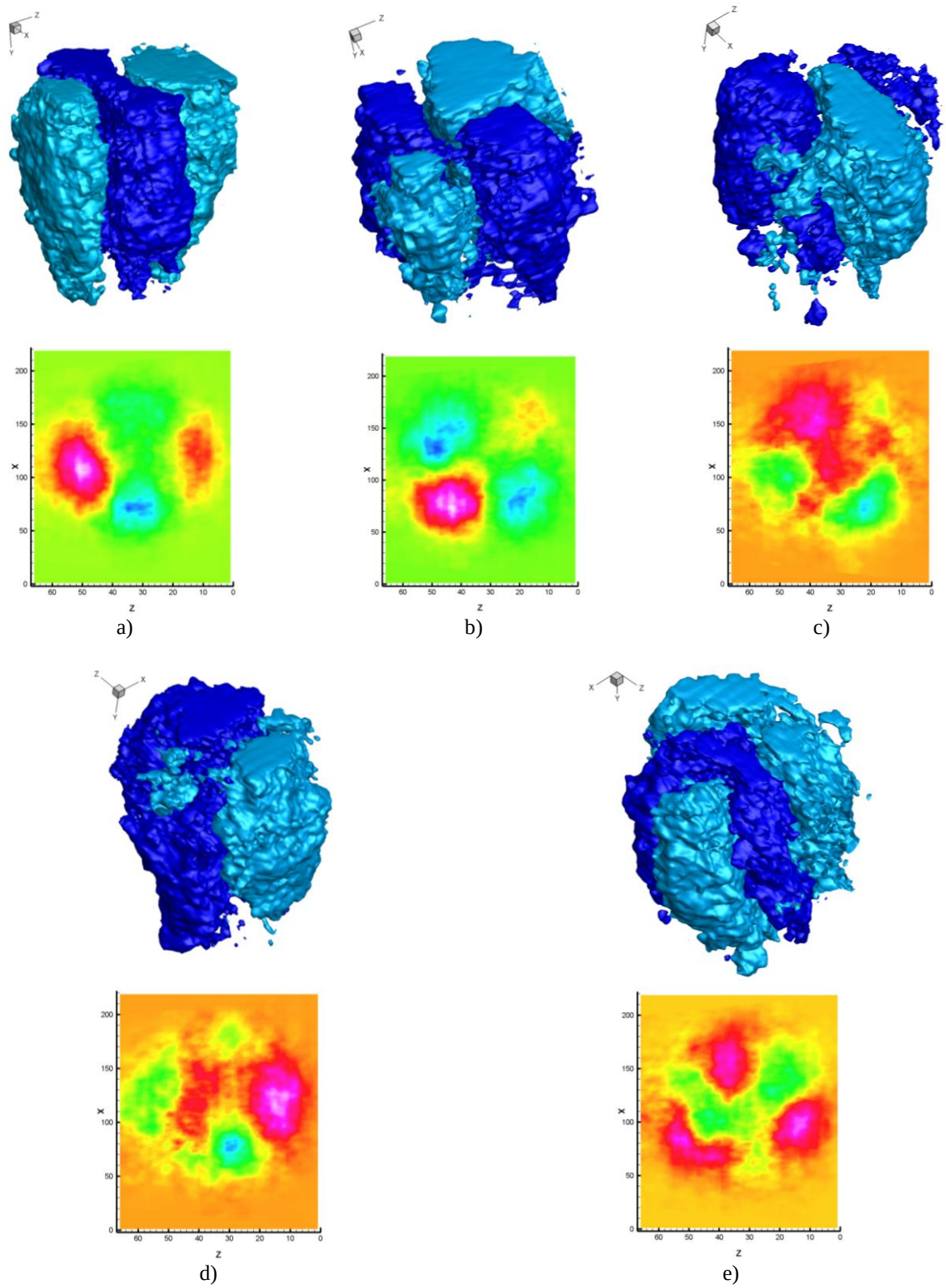

Figure 11: 3-D Iso-surface and 2-D central plane slice visualizations of near-field POD modes. a) mode 2, b) mode 3, c) mode 4, d) mode 5, e) mode 6. Note, the colormaps are not matched for the 3-D isosurface and the accompanying 2-D slice.

Modes 2-6 are shown in Figure 11, with accompanying cross-stream slices. Modes 2 and 3 represent a large scale flapping motion with a similar 90 degree rotation between modes that was seen in the near-field region. This allows the jet to flap in multiple directions. The remaining modes 4, 5, and 6 tend to represent a combination of flapping helical modes, where the jet has intertwining components in the streamwise direction. Again, we believe that some of the quality of these modes is degraded due to the image-by-image normalization procedure. However these results are promising, as they reveal structure in the jet that is not apparent in the instantaneous images.

IV. Conclusions

High-speed 3-D flow visualizations and an accompanying 3-D POD analysis were used to investigate the flow field in two regions of a circular jet. The general picture of the flow field formed from the 3-D images is consistent with that discussed in the literature [e.g. Refs. 1,2,4 & 9]. Near the nozzle exit, the shear layer instability results in the formation of ring vortices surrounding the jet core. As these vortices grow, azimuthal instabilities are clearly evident. The ring vortices eventually interact and collapse at the end of the potential core and begin transitioning to turbulent flow in our images of the transition region. The near-field behavior of the jet seems to be reflected in the instantaneous images which show ring vortices surrounded by finger-like fluid structure stretching in the streamwise direction and arranged in a quasiperiodic fashion around the annulus of the jet. Further downstream, in our transition region images, the dominant flow structure appears to take two different forms. The first is remnants of ring vortices (there is a slight overlap between the two regions studied), and a small expansion of the jet core.

POD analysis of the 3-D images provides an objective method to characterize some of the features observed in these images. POD modes of the near field clearly showed the vortex rings and modes in the transition region showed both ”flapping” and helical modes. At this stage, our results are best labeled as an ongoing effort to further describe jet structure using this unique 3-D imaging system. Further analysis is necessary to reduce the influence of artificial variances produced in image processing procedures and to piece together a complete picture of the flow field and to contrast it with what is known in the literature. The chain of events associated with transition to turbulence in jets is typically illustrated using cartoons; however, the use of 3-D flow visualization and POD may allow us to describe these events in more concrete terms. In addition, the content found in the higher order POD modes might illustrate some of the more subtle physics associated with this flow that might be difficult to observe or analyze through other means. This is particularly true as three-dimensional instabilities begin to play a more prominent role in the development and evolution of coherent structures.

In terms of future work, we are constantly improving our methodology as we seek to improve the quality of images acquired. This includes correcting improvements to normalization techniques and the refinement of ghosting corrections. The framework of these corrections is already established; however, in the case of normalization, the correction must be tuned for each data set, and for ghosting, a substantial data set is needed to accurately characterize the behavior of artifacts associated with the camera used in this study. The upgraded pulse burst laser is also providing us the flexibility to probe larger measurement volumes with greater pulse energy uniformity and beam quality. A new commercial smoke generator has also been ordered which should provide a constant seeding level throughout the course of the experiments.

With respect to further studies of the jet physics, as discussed in the introduction, we are interested in expanding our efforts to study the influence of excitation on the jet structure in the far-field. This will allow us to examine some of the fundamental questions of turbulence and demonstrate the utility of 3-D flow visualization for studies of turbulence. This is a planned effort that will build upon and utilize the experience gained in this effort. Another interesting area to explore is a comparison between POD modes formed from a set of 2-D images versus the set of 3-D images used in this work. This can be accomplished fairly easily by taking 2-D slices from the current data set and calculating the POD modes of the 2-D images. It will be interesting to see how the information in the modes compares from one set to the other

Acknowledgments

The support of the Army Research Office (program manager: Dr. Thomas Doligalski) through the Young Investigator Program is gratefully acknowledged. The authors would like to also acknowledge Andy Weldon for his help machining components for the laser system and jet facility, and Zach Reid for assistance in acquiring the data sets.

References

[1] Thurow, B. and Lynch, K., “3-D POD Analysis of a Naturally Excited Jet,” AIAA Paper 2008-4067, 2008.

[2] Dimotakis, P. E., "The mixing transition in turbulent flows," J. Fluid Mech., Vol. 409, pp 69-98, (2000).

[3] Crow, S.C. and Champagne, F.H., "Orderly structure in jet turbulence," J. Fluid Mech., Vol. 48, pp. 547-591, (1971).

[4] Yule, A.J., "Large-scale structure in the mixing layer of a round jet," J. Fluid Mech., Vol. 89, pp. 413-432, (1978).

[5] Ho, C-M. and Huange, L-S., "Subharmonics and vortex merging in mixing layers," J. Fluid Mech., Vol. 119, pp. 443-473, (1982).

[6] Dimotakis, P.E., Miake-Lye, R.C. and Papantoniou, D.A., "Structure and dynamics of round turbulent jets," Phys. Fluids, Vol. 26, pp. 3185-3192, (1983).

[7] Husain, Z.D. and Hussain, A.K.M.F., "Natural instability of free shear layers," AIAA J., Vol. 21, pp. 1512-1517, (1983).

[8] Gutmark, E. and Ho C-M., "Preferred modes and the spreading rates of jets," Phys. Fluids, Vol. 26, pp. 2932-2938, (1983).

[9] Ho, C-M. and Huerre, P., "Perturbed free shear layers," Annu. Rev. Fluid Mech., Vol. 16, pp. 365-424, (1984).

[10] Samet, M.M. and Petersen, R.A., "Effects of excitation level on the stability of an axisymmetric mixing layer," Phys. Fluids, Vol. 31, pp. 3246-3252, (1988).

[11] Liepmann, D. and Gharib, M., "The role of streamwise vorticity in the near-field entrainment of round jets," J. Fluid Mech., Vol. 245, pp. 643-668, (1992).

[12] Corke, T.C. and Kusek, S.M., "Resonance in axisymmetric jets with controlled helical-mode input," J. Fluid Mech., Vol. 249, pp. 307-336, (1993).

[13] Verzicco, R. and Orlandi, P., "Direct simulations of the transitional regime of a circular jet," Phys. Fluids, Vol. 6, pp. 751-759, (1994).

[14] Wicker, R.B. and Eaton, J.K., "Near field of a coaxial jet with and without axial excitation," AIAA J., Vol. 32, pp. 542-546, (1994).

[15] Cho, S. K., Yoo, J.Y. and Choi, H., "Vortex pairing in an axisymmetric jet using two-frequency acoustic forcing at low to moderate strouhal numbers," Exp. Fluids, Vol 25, pp. 305-315, (1998).

[16] Oh, S.K. and Shin, H.D., "A visualization study on the effect of forcing amplitude on tone-excited isothermal jets and jet diffusion flames," Int. J. Energy Res., Vol. 22, pp. 343-354, (1998).

[17] Schram, C. and Rietmuller, M.L., "Measurement of vortex ring characteristics during pairing in a forced subsonic air jet," Exp. Fluids, Vol. 33, pp. 879-888, (2002).

[18] Olsen, J.F., Rajagopalan, S. and Antonia, R.A., "Jet column modes in both a plane jet and a passively modified plane jet subject to acoustic excitation," Exp. Fluids, Vol. 35, pp. 278-287, (2003).

[19] Reynolds, W.C., Parekh, D.E., Juvet, P.J.D. and Lee, M.J.D., "Bifurcating and blooming jets," Annu. Rev. Fluid Mech., Vol. 35, pp. 295-315, (2003).

[20] Tinney, C.E., Glauser, M. N., and Ukeiley, L.S., "The evolution of the most energetic modes in a high subsonic Mach number turbulent jet," AIAA Paper 2005-0417, 43rd AIAA Aerospace Sciences Meeting and Exhibit, January 2005.

[21] Birbaud, A.L., Durox, D., Ducruix, S. and Candel, S., "Dynamics of free jets submitted to upstream acoustic modulations," Phys. Fluids, Vol. 19, 013602, (2007).

[22] Iqbal, M.O. and Thomas, F.O., "Coherent structure in a turbulent jet via a vector implementation of the proper orthogonal decomposition," J. Fluid Mech., Vol. 571, pp. 281-326, (2007).

[23] Sirovich, L., "Turbulence and the dynamics of coherent structures. Part 1: Coherent structures," Quarterly of App. Math., Vol. XLV, pp. 561-571, (1987).

[24] Berkooz, G., Holmes, P. and Lumley, J.L., "The proper orthogonal decomposition in the analysis of turbulent flows," Annu. Rev. Fluid Mech., Vol. 25, pp. 539-575, (1993).

[25] Everson, R. and Sirovich, L., "Karhunen-Loeve procedure for gappy data," J. Opt. Soc. Am. A, Vol. 12, pp. 1657-1664, (1995).

[26] Holmes, P.J., Lumley, J.L., Berkooz, G, Mattingly, J.C. and Wittenberg, R.W., "Low-dimensional modes of coherent structures in turbulence," Physics Reports, Vol. 287, pp. 337-384, (1997).

[27] Chatterjee, A., "An introduction to the proper orthogonal decomposition," Current Science, Vol. 78, pp. 808-817, (2000).

[28] Smith, T.R., Moehlis, J. and Holmes, P., "Low-dimensional modeling of turbulence using the proper orthogonal decomposition: A tutorial," Nonlinear Dynamics, Vol. 41, pp. 275-307, (2005).

[29] Thurow, B., and Lynch, K., "Development of a High-Speed Three Dimensional Flow Visualization Technique," accepted for publication in *AIAA J.*, October 2008.

[31] Thurow, B., Satija, A., and Lynch, K., "Third-generation megahertz-rate pulse burst laser system," *Applied Optics*, Vol. 48, pp. 2086-2093, (2008).

[32] Jiang, N., Webster, M., and Lempert, W., "Advances in the generation of high-repetition-rate burst mode laser output," *Applied Optics*, Vol. 48, pp. B23-B31, (2009).